DOI https: //doi. org/10.1007/s11595-022-2599-7

# Preparation of $Bi_2O_3$/BiOI Step-scheme Heterojunction Photocatalysts and Their Degradation Mechanism of Methylene Blue

**JIANG Xuechao[1], TAN Haiyan[1,2,3*], SHI Xinyu[1], CHENG Xinhua[1], HU Weibing[1], HU Xinhui[1]**

*(1. Key Laboratory of Green Manufacturing of Super-light Elastomer Materials of State Ethnic Affairs Commission, School of Chemistry and Environmental Engineering, Hubei Minzu University , Enshi 445000, China; 2. Guangxi Key Laboratory of Chemistry and Engineering of Forest Products, Guangxi University for Nationalities, Nanning 530006, China; 3. State Key Laboratory of Advanced Technology for Materials Synthesis and Processing, Wuhan University of Technology, Wuhan 430070, China)*

**Abstract:** $Bi_2O_3$/BiOI step-scheme(S-scheme) heterojunction photocatalyst was synthesized by green calcination method, its degradation ability of methylene blue was investigated, and the photocatalytic performance of the $Bi_2O_3$/BiOI heterojunction, $Bi_2O_3$ and BiOI was compared. The structure and morphology of the samples were characterized by X- ray diffraction(XRD), field emission scanning electron microscopy (FESEM), and UV-vis diffuse reflection spectrum (UV-vis DRS). The degradation rate of methylene blue was analysised by spectrophotometry, and the calculation result showed that the degradation rate of methylene blue was 97.8% in 150 minutes. The first order kinetic rate constant of 10%$Bi_2O_3$/BiOI is 0.021 8 $min^{-1}$, which are 2.37 and 2.68 times of BiOI(0.009 18 $min^{-1}$) and $Bi_2O_3$ (0.008 03 $min^{-1}$) respectively. The calculation result shows that the work function of $Bi_2O_3$ and BiOI are 3.0 eV and 6.0 eV, respectively, by density functional theory(DFT). When this S-scheme heterojunction is used as a photocatalyst, the weaker electrons in the conduction band of BiOI will be combined with the weaker holes in the $Bi_2O_3$ valence band under combined effect with built-in electric field and band bending, which will retain stronger photoelectrons and holes between $Bi_2O_3$ and BiOI. This may be the internal reason for the efficient degradation of tetracycline by $Bi_2O_3$/BiOI S-scheme heterostructures.

**Key words:** step-scheme heterojunction; methylene blue; antibiotic wastewater treatment; photocatalytic degradation; charge separation

## 1 Introduction

Semiconductor photocatalysis is considered as a promising approach to solve the current energy shortage and environmental pollution problems, therefore a great number of efforts have focused on developing semiconductor photocatalysts. Among them, photocatalyst materials has been used in photocatalysis field, including photocatalytic removal of heavy metal ion such as elemental mercury[1], photocatalytic $H_2$ generation[2], photocatalytic $CO_2$ reduction[3], photocatalytic removal herbicide[4], recycling of electric arc furnace dust[5], degradation of pharmaceutical waste water, such as tetracycline[6], photocatalysis sterilization[7], and photocatalytic degradation of organic matter. Photocatalysis can sustainably convert inexhaustible solar energy into storable chemical energy. It is environmentally friendly due to its low energy input and carbon footprint.

Photocarriers of single photocatalyst are easy to be compounded, and the construction of a traditional type II heterojunction is a common and effective strategy to realize the photoelectron and hole separation. Type II heterojunction can effectively separate electron-hole, but it weakens the reduction and oxidation ability of electron-hole. To solve low reduction and



(Received: Nov. 29, 2021; Accepted: June 15, 2022)

JIANG Xuechao(姜雪超): E-mail: 2475111028@qq.com

*Corresponding author:TAN Haiyan(谭海燕): Ph D; Assoc. Prof.; E-mail: 414384126@qq.com

Funded by National Natural Science Foundation of China (No.21769009), Project of Innovation and Entrepreneurship for College Students in Hubei Minzu University (No.S202010517044), The foundation of Key Laboratory of Green Manufacturing of Super-light Elastomer Materials of State Ethnic Affairs Commission. (Hubei Minzu University)(No.PT092101), The Open Project of Guangxi Key Laboratory of Chemistry and Engineering of Forest Products(No.GXFK1904), and Specific Research Project of Guangxi for Research Bases and Talents(No.AD18126005)

oxidation abilities in type II heterojunctio, S-Scheme heterojunction was invented by the researchers[8,9]. The built-in electric field, band edge bending, and coulomb interaction synergistically facilitated the recombination of relatively useless electrons and holes in hybrid when the interface was irradiated by simulated solar light. Therefore, the remaining electrons and holes with higher reducibility and oxidizability endowed the composite with supreme redox ability[10].

Dye degradation is a typical photocatalytic degradation of organic compounds. Landge *et al*[11] synthesised a novel S-scheme $Bi_2O_3$-ZnO on bentonite clay nanocomposite for the degradation of congo red (CR). Liu *et al*[12] prepared S-scheme heterojunction ZnO/g-$C_3N_4$ shielding polyester fiber composites for the degradation of MB. Gogoi *et al*[13] prepared S-scheme heterojunction $CoFe_2O_4$-g$C_3N_4$ for the degradation of model dyes and industrial dyes. It is obvious that S-scheme heterojunction plays an important role in dye wastewater treatment. However, the wide band gap of them, instinctive recombination of photoinduced carriers, and other defects result in its low solar quantum efficiency and restrict its practical utility. It is an effective method to construct S-scheme heterojunction by finding materials with narrow-band-gap. In photocatalyst it is easy to form lamellar structure in the synthesis of Bismuth halide oxide BiOX(X= Cl, Br, I). It is easy to form alternating structure between $[Bi_2O_2]^{2+}$ and $X^-$ and then to form built-in electric field, which can further promote the separation of photoelectrons and holes. This makes bismuth halides have a great number of application prospect in photocatalytic degradation. The band gap of BiOI is the narrowest (about 1.7-1.9 eV) in BiOX, but its absorption range is wide, including almost all visible light (about 400-700 nm), and its high stability, and strong oxidizing ability, has attracted considerable attention[14]. However photoelectrons and holes in a single BiOI are easy to recombine. Tan *et al*[15] prepared S-scheme heterojunction BiOBr/BiOI for the degradation of rhodamine B. It showed that the degradation rate of rhodamine B was 100% in forty minutes. It is obvious that S-scheme heterojunction of BiOX/BiOX have excellent degradation properties in dye wastewater treatment, but there have been few reports in this field.

In order to study the photocatalytic degradation ability of BiOX S-scheme heterojunctions and overcome the shortcoming of easy recombination of photoelectrons and holes in a single BiOI, we have constructed S-scheme heterojunctions with level-matched semiconductors $Bi_2O_3$ and BiOI. $Bi_2O_3$/BiOI heterojunction composite catalytic material was synthesized by hydrothermal method. Its degradation ability of methylene blue was investigated, and the photocatalytic performance of the $Bi_2O_3$/BiOI heterojunction, $Bi_2O_3$ and BiOI was compared. Density functional theory (DFT) was applied to evaluate and calculate the band structure[16,17], density of states and electrostatic potential. The degradation mechanism of $Bi_2O_3$/BiOI heterojunction material to methylene blue was discussed based on DFT and XPS, which will provide a meaningful reference for the green degradation of high concentration organic dyes.

## 2 Experimental

### 2.1 Synthesis of photocatalyst

2.1.1 Preparation of BiOI and $Bi_2O_3$

Typically, 19.40 g (0.04 mol) $Bi(NO_3)_3{\cdot}5H_2O$ were dispersed in 60 mL of glacial acetic acid under ultrasonic conditions. 6.4 g (0.04 mol) KBr were dispersed in 650.00 mL deionized water. Subsequently, $Bi(NO_3)_3{\cdot}5H_2O$ solution was added to the KBr solution with magnetic stirring for 3 h at 80℃. After the reaction, the obtained sample was centrifuged at 5 000 rpm for 3 min, washed with deionized water and absolute ethanol, and dried at 60 ℃ for 12 h. $Bi_2O_3$ was prepared by calcining Bi $(NO_3)_3{\cdot}5H_2O$ at 600 ℃.

2.1.2 Preparation of $Bi_2O_3$/BiOI

1.700 4 g $Bi(NO_3){\cdot}5H_2O$ were dispersed in 60 mL of glacial acetic acid under ultrasonic conditions. 7.020 1 g BiOI were dispersed in 30 mL deionized water under ultrasonic conditions. Subsequently, $Bi(NO_3)_3{\cdot}5H_2O$ solution was added to the KBr solution with magnetic stirring for 1-2 h. Then the obtained sample was centrifuged at 5 000 rpm for 3 min, washed with deionized water, and dried at 60 ℃ for 12 h. Finally the sample was prepared by calcining at 600 ℃. The samples were labeled as 10% $Bi_2O_3$/BiOI, then 5% $Bi_2O_3$/BiOI and 20% $Bi_2O_3$/BiOI composites were prepared by the same method.

### 2.2 Characterization

The microstructure investigation of the as-prepared samples were taken on a field emission scanning electron microscope (FESEM) (JSM 7500F, JEOL, Japan). The crystal structure of the catalysts was analyzed by X-ray diffractometer (XRD-6100, Shimadzu, Japan). X-ray photoelectron spectroscopy (XPS) measurements were performed by an Escalab 250Xi X-ray photo-electron spectroscope (Thermo Fisher Scientific, USA) with a monochromatic Al K$\alpha$ X-ray source. Room temperature UV-vis absorption spectrum was obtained by a UV-vis spectrophotometer

(UV -1240, Shimadzu, Japan).

### 2.3 Photocatalytic degradation of methylene blue

To evaluate the photocatalytic performance of various samples, methylene blue was used as the organic to conduct the degradation experiments under the light irradiation. Concretely, 0.050 0 g of catalyst was added to 100 mL of methylene blue aqueous solution (10 mg/L) in a glass reactor. The mixture was magnetically stirred in the dark for 30 min to establish the adsorption/desorption equilibrium. A 300 W Xe lamp (Yinzhu, Zhenjiang) was employed as the light source. When the Xe lamp was turned on, 5 mL of suspension was taken out at intervals of 10 min, and then it was centrifuged to remove the powder catalyst. The filtrate absorbance was measured by a UV- Vis spectrophotometer (UV mini-1240, Shimadzu, Japan) at 663 nm which is the wavelength for maximum absorption of methylene blue. The methylene blue degradation process was monitored by the $C_t/C_0$ ratio, where $C_t$ and $C_0$ refer to absorbance of filtrates at different reaction times and absorbance of the initial methylene blue aqueous solution, respectively.

## 3 Results and discussion

### 3.1 XRD analysis

The photocatalyst structures of pure $Bi_2O_3$, $Bi_2O_3$/BiOI and BiOI were investigated by X-ray diffraction (XRD) patterns. As shown in Fig.1, the diffraction peaks of $Bi_2O_3$ is consistent with that of $Bi_2O_3$ reported in literature[18]. Its characteristic peaks at 25.8°and 28.1°belong to (001) and (012) planes (JCPDS No. 71-0465), which indicates that the bulk synthesized material is homogeneous and its relative phase is monoclinic. At the same time, the diffraction peaks of BiOI agree with the XRD pattern of BiOI in references[19]. Its characteristic peaks at 9.7°and 29.7°belong to (001) and (012) planes (JCPDS No. 73-2062). The main diffraction peak positions of $Bi_2O_3$/BiOI heterojunction materials are consistent with those of $Bi_2O_3$ and BiOI, indicating that $Bi_2O_3$/BiOI composite photocatalyst has been synthesized.

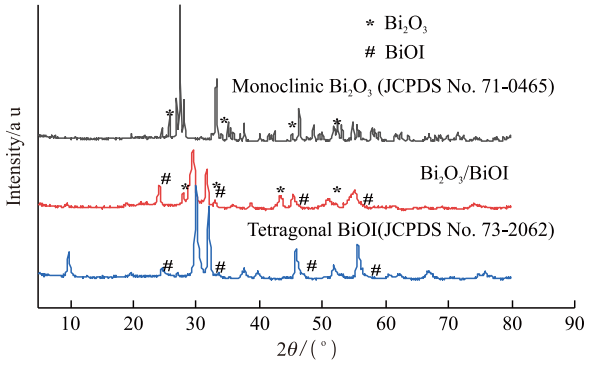


Fig.1 XRD pattern of different catalysts

### 3.2 SEM analysis

The microscopic morphologies of the as-prepared pure BiOI, $Bi_2O_3$ and $Bi_2O_3$/BiOI, and the corresponding images are shown in Fig.2. Pure BiOBr possessed a peonies-like spherical lamellar structure, pure $Bi_2O_3$ showed a special cube structure, and pure $Bi_2O_3$/BiOI showed a special lamellar structure. This indicates that $Bi_2O_3$ particles were successfully loaded onto BiOI lamellae by reaction.

### 3.3 UV-vis diffuse reflection spectrum analysis

The UV-vis adsorption spectra of the synthetic materials are shown in Fig.3. Pure $Bi_2O_3$ shows a steep absorption edge at 462 nm, the edge of $Bi_2O_3$/BiOI is located at approximately 595 nm, and the edge of BiOI is located at approximately 702 nm. The energy gap of the photocatalyst is calculated by Eq.(1):

$$\alpha h\nu = A(h\nu - E_g)^{n/2} \quad (1)$$

where, $\alpha$, $\nu$, $h$, $E_g$, and $A$ represent the absorption coefficient, light efficiency, planck constant, band- gap energy, and proportional constant, respectively[20,21]. The value of $n$ is 4 for both BiOI and $Bi_2O_3$ because they are indirect transition semiconductors. Based on the above formula, $E_g$ is 2.68 eV for $Bi_2O_3$ and 1.77 eV for BiOI. The positions of the conduction band ($E_{CB}$) and valence band ($E_{VB}$) are estimated by Eqs.(2) and (3):

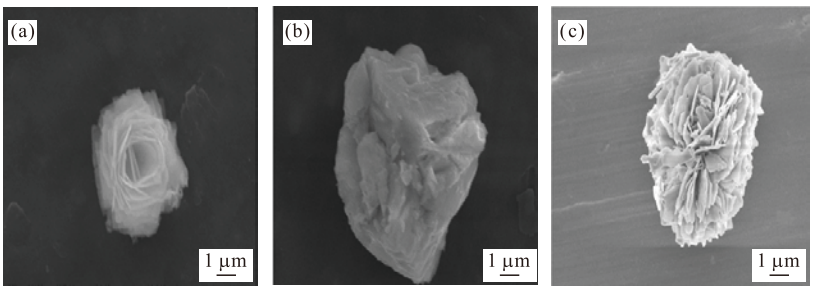


Fig.2 SEM images of catalysts: (a) BiOI; (b) $Bi_2O_3$; (c) $Bi_2O_3$/BiOI

$$E_{CB} = \chi - E^e - 0.5\,E_g \quad (2)$$

$$E_{VB} = E_g + E_{CB} \quad (3)$$

where, $\chi$ is the geometric mean of the absolute electronegativity of the constituent atoms. $E^e$ is a constant (approximately 4.5 eV) corresponding to the energy of free electrons on the hydrogen scale. The $E_{CB}$ and $E_{VB}$ are calculated to be 0.56 and 2.33 eV respectively for BiOI, and the $E_{CB}$ and $E_{VB}$ are calculated to be −0.65 and 2.03 eV respectively for $Bi_2O_3$.

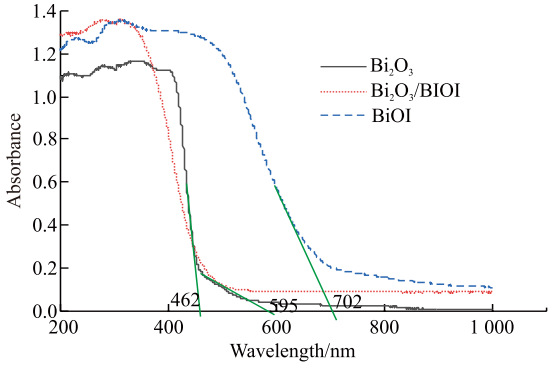


Fig.3 UV-vis adsorption spectra of the synthetic materials

## 3.4 Photocatalytic performance analysis

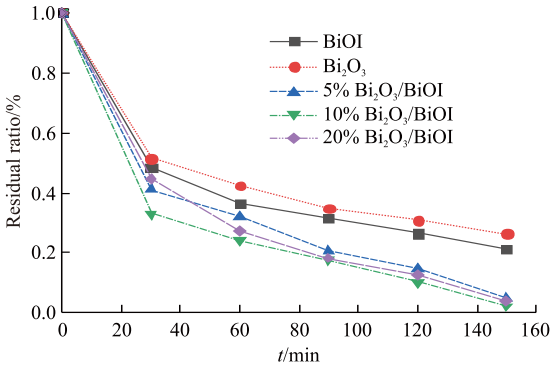


Fig.4 Photocatalytic degradation of methylene blue (10 mg/L) solution with different catalysts

Photocatalytic degradation effect of methylene blue (10 mg/L) solution with different catalysts are exhibited in Fig.4. After 2.5 hours of photocatalytic reaction, the residual rates of BiOI, $Bi_2O_3$, 5%$Bi_2O_3$/BiOI, 10%$Bi_2O_3$/BiOI, 20%$Bi_2O_3$/BiOI were 21.5%, 26.3%, 4.9%, 2.2%, and 3.9% respectively. The results show that the $Bi_2O_3$/BiOI heterojunction photocatalytic materials have good degradation ability to 10 mg/L methylene blue, which was also significantly higher than the degradation rate of pure $Bi_2O_3$ and BiOI. The kinetic equation was further utilized to evaluate the photocatalytic degradation activity of methylene blue, and the result are shown in Fig.5. The reaction rate ($k$) depends on the slope of the pseudo-first-order kinetic equation: $\ln(C_0/C_t) = kt$, where $C_t$ and $C_0$ represent the concentration of methylene blue at light irradiation times of $t$ min and 0 min, respectively. The rate constants of BiOI, $Bi_2O_3$, 5% $Bi_2O_3$/BiOI, 10% $Bi_2O_3$/BiOI and 20% $Bi_2O_3$/BiOI were calculated to be 0.009 18, 0.008 03, 0.017 7, 0.021 8, and 0.019 4 $min^{-1}$ respectively. The first order kinetic rate constant of 10%$Bi_2O_3$/BiOI was 0.021 8 $min^{-1}$, which are 2.37 and 2.68 times of BiOI(0.009 18 $min^{-1}$) and $Bi_2O_3$ (0.00803 $min^{-1}$), respectively.

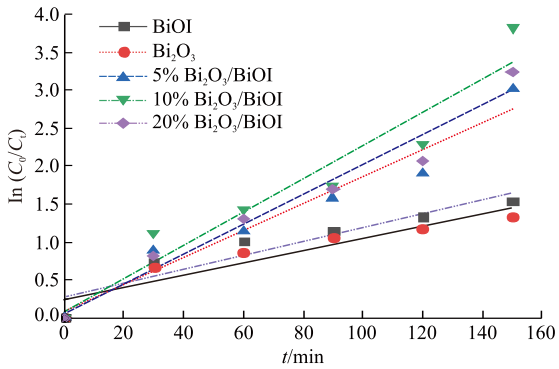


Fig.5 First-order kinetic fitting of the photodegradation of methylene blue with different catalysts

## 3.5 Determination of active species

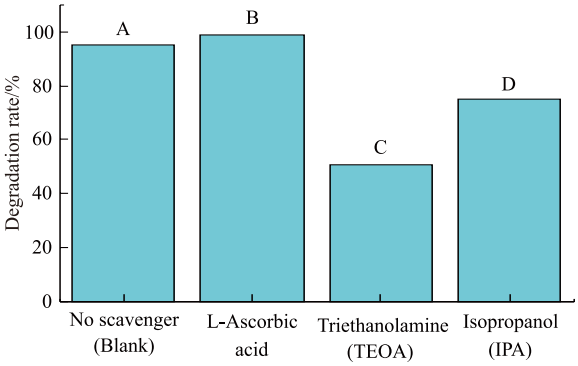


Fig.6 Species trapping experiments of the synthetic material during methylene blue degradation

The active species-trapped experiments were performed under the standard methylene blue photodegradation conditions. As shown in Fig.6, triethanolamine(TEOA), isopropanol(IPA), L-ascorbic acid were used to trap holes ($h^+$), hydroxyl radicals (•OH), and superoxide radicals ($\bullet O_2^-$), respectively. The result indicates the degradation efficiency of methylene blue did not change in the presence of L-ascorbic acid. But after adding TEOA and IPA, the degradation efficiency obviously decreased. The results indicated that •OH and $h^+$ were active species whereas $\bullet O_2^-$ was

not. In particular, $h^+$ played a more important role than •OH, showing that $h^+$ was the main active species during the photodegradation of the methylene blue solution.

### 3.6 Calculation of electrostatic potential of photocatalytic materials

3.6.1 Calculation methods

The density functional theory (DFT) calculations were conducted through the VASP module in Materials Studio software. The 001 surfaces of $Bi_2O_3$ and BiOI are used as computational models respectively. As shown in Fig.7, when performing geometric optimization, the energy cut-off is set to 500 eV, and the *k*-point grid is set to 6 × 6 × 3 in all the models. The maximum force exerted on the atom is 0.03 eV/Å. The convergence criterion is set to $1.0\times10^{-4}$ eV /atomic energy. In building the surface model, a vacuum layer of 20 Å is used to eliminate the surface interaction in the *Z* direction. The crystal structure of BiOI and $Bi_2O_3$ are shown in Fig.7.

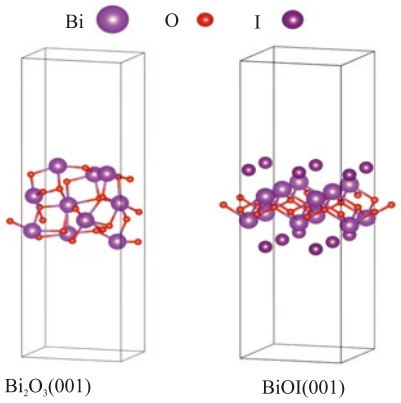


Fig.7 Calculation model diagram of $Bi_2O_3$ and BiOI

3.6.2 Electrostatic potential of $Bi_2O_3$ and BiOI

The electrostatic potential of $Bi_2O_3$(001) and BiOI (001) are shown in Fig.8, and their work function are 3.0 and 6.0 eV respectively. Obviously the work function of $Bi_2O_3$ is smaller than that of BiOI, but its Fermi level is larger than that of BiOI's Fermi level. During the photocatalysis reaction, some electrons are transferred from the $Bi_2O_3$ semiconductor to the BiOI semiconductor under such a large Fermi energy level difference. Thus opposite charges are accumulated on both sides of the interface to form a directional built-in electric field from $Bi_2O_3$ to BiOI. Under the influence of the built-in electric field the potential of $Bi_2O_3$ will increase and the potential of BiOI will decrease. The band edge of $Bi_2O_3$ is bending up and the band edge of BiOI is bending down. Combined with the previous calculation we know the conduction band and valence band of BiOI are 0.56 and 2.33 eV respectively, and the conduction band and valence band of $Bi_2O_3$ are −0.65 and 2.03 eV respectively. So it is concluded that $Bi_2O_3$ and BiOI can form S-scheme heterojunction.

### 3.7 Possible photocatalytic mechanism

Fig.9 shows the charge transfer mechanism of the S-scheme heterojunction between $Bi_2O_3$ and BiOI. Since the work function of $Bi_2O_3$ is 3.0 eV, its conduction band and valence band are −0.65 and 2.03 eV respectively. However the work function of BiOI is 6.0 eV, and its conduction band and valence band are 0.56 and 2.33 eV respectively. When the two semiconductors form a S-scheme heterojunction, some electrons are transferred from the $Bi_2O_3$ semiconductor to the BiOI semiconductor until the Fermi energy levels of both are close to equilibrium. Under the influence of the built-in electric field the potential of $Bi_2O_3$ will increase and the potential of BiOI will decrease, and the band edge of $Bi_2O_3$ is bending up and the band edge of BiOI is bending down. Benefiting from the internal electric field, band edge bending, and coulomb interaction, the relatively weaker BiOI CB electrons and $Bi_2O_3$ VB holes are quenched, but the $Bi_2O_3$ CB electrons and BiOI VB holes with the stronger redox abilities remain. Therefore, this electron transfer process endows the hybrid with a supreme redox capacity and has been confirmed by the radical trapping experiments. It was confirmed that both hole ($h^+$) and hydroxyl radical (•OH) play an important role in the photocatalytic degradation of methylene blue.

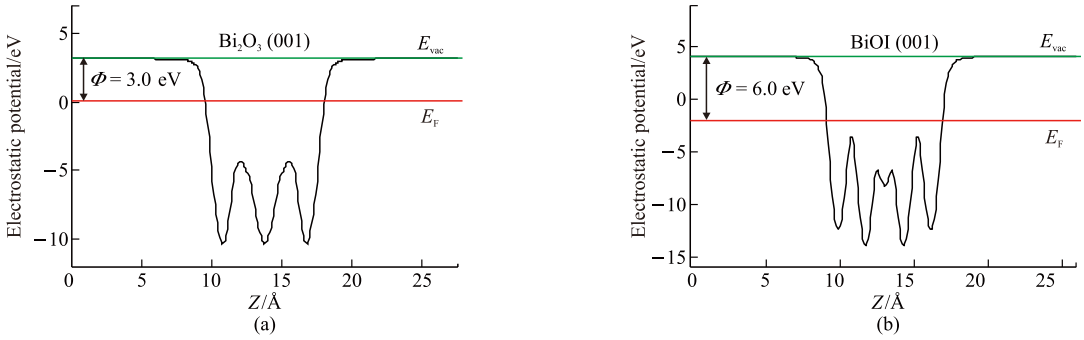


Fig.8 The electrostatic potential of $Bi_2O_3$ (001) and BiOI (001)

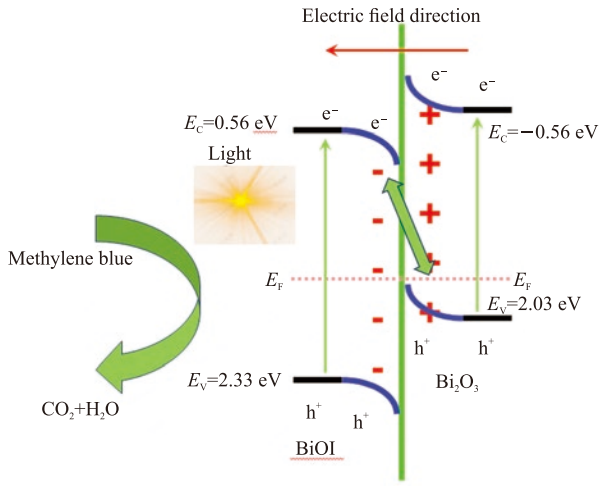


Fig.9 The possible photocatalytic mechanism of methylene blue

# 4 Conclusions

A new type S-scheme heterojunction photocatalyst $Bi_2O_3$/BiOI was prepared by a green method for the degradation of methylene blue in dye wastewater. The photocatalytic performance of the $Bi_2O_3$/BiOI heterojunction, $Bi_2O_3$ and BiOI was compared. The $Bi_2O_3$/BiOI heterojunction photocatalytic materials have good degradation ability to 10 mg/L methylene blue. It showed that the degradation rate of methylene blue was 97.8% in 150 minutes, which was also significantly higher than that of pure $Bi_2O_3$ and BiOI. The first order kinetic rate constant of 10%$Bi_2O_3$/BiOI is 0.021 8 $min^{-1}$, which are 2.37 and 2.68 times of BiOI (0.009 18 $min^{-1}$) and $Bi_2O_3$ (0.008 03 $min^{-1}$) respectively. $Bi_2O_3$/BiOI S-scheme heterojunction photocatalyst had a good spherical lamellar structure, which was beneficial to the separation of electron holes in the S-scheme heterojunction. The active species-trapped experiments show that the hole ($h^+$) and hydroxyl radical (•OH) play a strong oxidation role in the degradation of methylene blue. The calculation result of the DFT show that $Bi_2O_3$ and BiOI can form S-scheme heterojunction. The results show that S-scheme heterojunction is more advantageous to retain the reduced semiconductor CB electrons and oxide semiconductor VB holes with the stronger redox abilities. In a word this heterojunction photocatalyst can not only effectively promote the photogenerated charge separation but also maintain the strong redox ability of the composites, which may be the internal reason for the efficient degradation of methylene blue by $Bi_2O_3$/BiOI heterostructures. This study is helpful to understand the excellent activity of S-scheme heterojunction photocatalytic in the degradation of organic compounds in dye wastewater.

## References


[1] Alshaikh H, Al-Hajji L A, Mahmoud M H, *et al.* Visible-Light-Driven S-scheme Mesoporous $Ag_3VO_4/C_3N_4$ Heterojunction with Promoted Photocatalytic Performances[J]. *Sep. Purif. Technol.*, 2021, 272: 118 914

[2] Liu Q Q, He X D, Peng J J, *et al*. Hot-Electron-Assisted S-Scheme Heterojunction of Tungsten Oxide/Graphitic Carbon Nitride for Broad-Spectrum Photocatalytic $H_2$ Generation[J]. *Chinese J. Catal.*, 2021, 42: 1 478-1 487

[3] Zhang T, Maihemllti M, Okitsu K J, *et al*. *In Situ* Self-Assembled S-Scheme BiOBr/PCN Hybrid with Enhanced Photocatalytic Activity for Organic Pollutant Degradation and $CO_2$ Reduction[J]. *Appl. Surf. Sci.*, 2021, 556: 149 828

[4] Enesca A, Isac L. Tuned S-Scheme $Cu_2S$-$TiO_2$-$WO_3$ Heterostructure Photocatalyst Toward S-Metolachlor (S-MCh) Herbicide Removal[J]. *Materials*, 2021, 14: 2 231

[5] Kamali M, Sheibani S, Ataie A. Magnetic $MgFe_2O_4$- $CaFe_2O_4$ S-Scheme Photocatalyst Prepared from Recycling of Electric Arc Furnace Dust[J]. *J. Environ. Manage.*, 2021, 290: 112 609

[6] Zhang K, Li D Q, Tian Q Y, *et al*. Recyclable 0D/2D $ZnFe_2O_4/Bi_5FeTi_3O_{15}$ S-Scheme Heterojunction with Bismuth Decoration for Enhanced Visible-Light-Driven Tetracycline Photodegradation[J]. *Ceram. Int.*, 2021, 47: 17 109-17 119

[7] Yousefi S R, Ghanbari M, Amiri O, *et al.* $Dy_2BaCuO_5/Ba_4DyCu_3O_{9.09}$ S-Scheme Heterojunction Nanocomposite with Enhanced Photocatalytic and Antibacterial Activities[J]. *J. Am. Ceram. Soc*., 2021, 104: 2 952-2 965

[8] Li J K, Li M, Jin Z L. Rational Design of a Cobalt Sulfide/Bismuth Sulfide S-Scheme Heterojunction for Efficient Photocatalytic Hydrogen Evolution[J]. *J. Colloid. Interf. Sci*, 2021, 592: 237-248

[9] Liu Y, Hao X Q, Hu H Q, *et al.* High Efficiency Electron Transfer Realized over $NiS_2/MoSe_2$ S-Scheme Heterojunction in Photocatalytic Hydrogen Evolution[J]. *Acta. Phys. -Chim. Sin*., 2021, 37 (6): 2 008 030

[10] Wang J, Wang G H, Cheng B, *et al*. Sulfur-Doped g-$C_3N_4/TiO_2$ S-Scheme Heterojunction Photocatalyst for Congo Red Photodegradation[J]. *Chinese J. Catal.*, 2021, 42: 56-68

[11] Landge V K, Sonawane S H, Sivakumar M, *et al.* S-Scheme Heterojunction $Bi_2O_3$-ZnO/Bentonite Clay Composite with Enhanced Photocatalytic Performance[J]. *Sustain. Energy Techn*., 2021, 45: 101 194

[12] Liu X Y, Li J. S-Scheme Heterojunction ZnO/g-$C_3N_4$ Shielding Polyester Fiber Composites for the Degradation of MB[J]. *Semicond. Sci. Tech.*, 2021, 36: 045 025

[13] Gogoi D, Makkar P, Ghosh N N. Solar Light-Irradiated Photocatalytic Degradation of Model Dyes and Industrial Dyes by a Magnetic $CoFe_2O_4$- $gC_3N_4$ S-Scheme Heterojunction Photocatalyst[J]. *ACS Omega.*, 2021, 6: 4 831- 4 841

[14] Zhang B, Hu X Y, Liu E Z, *et al.* Novel S - scheme 2D/2D BiOBr/g-$C_3N_4$ Heterojunctions with Enhanced Photocatalytic Activity[J]. *Chinese J. Catal.*, 2021, 42: 1 519-1 529

[15] Tan H Y, Zhang S L, Wu D Y, *et al.* Preparation of BiOI/BiOBr Heterojunction Catalyst and Its Photocatalytic Degradation of Rhodamine B[J]. *Journal of Huanzhong Agricultural University*, 2021, 40(3): 187-194

[16] Chen X, Ke X C , Zhang J F, *et al*. Insight into the Synergy of Amine-Modified S-Scheme $Cd_{0.5}Zn_{0.5}Se$/porous g-$C_3N_4$ and Noble-Metal- Free $Ni_2P$ for Boosting Photocatalytic Hydrogen Generation[J]. *Ceram. Int*., 2021, 47: 13 488-13 499

[17] Chen X, Hu T P, Zhang J F, *et al*. Diethylenetriamine Synergistic Boosting Photocatalytic Performance with Porous g-$C_3N_4$/CdS - Diethylenetriamine 2D/2D S-Scheme Heterojunction[J]. *J. Alloy Compd.*, 2021, 863: 158 068

[18] Duan F, Ma Y, Lv P, *et al.* Oxygen Vacancy-Enriched $Bi_2O_3/BiFeO_3$ p-n Heterojunction Nanofibers with Highly Efficient Photocatalytic Activity Under Visible Light Irradiation[J]. *Appl. Surf. Sci*., 2021, 562: 150 171

[19] Zhang H L, Li M, Wang W, *et al*. Designing 3D Porous BiOI/$Ti_3C_2$ Nanocomposite as a Superior Coating Photocatalyst for Photodegradation RhB and Photoreduction Cr (VI)[J]. *Sep. Purif. Technol*, 2021, 272: 118 911

[20] Cao Y, Wang G R, Liu H, *et al*. Regular Octahedron Cu-MOFs Modifies $Mn_{0.05}Cd_{0.95}S$ Nanoparticles to Form a S-Scheme Heterojunction for Photocatalytic Hydrogen Evolution[J]. *Int. J. Hydrogen. Energ*., 2021, 46: 7 230-7 240

[21] Li J K, Li M, Jin Z L. 0D $Cd_xZn_{1-x}S$ and Amorphous $Co_9S_8$ Formed S-Scheme Heterojunction Boosting Photocatalytic Hydrogen Evolution[J]. *Mol. Catal.*, 2021, 501: 111 378